Dam Engineering

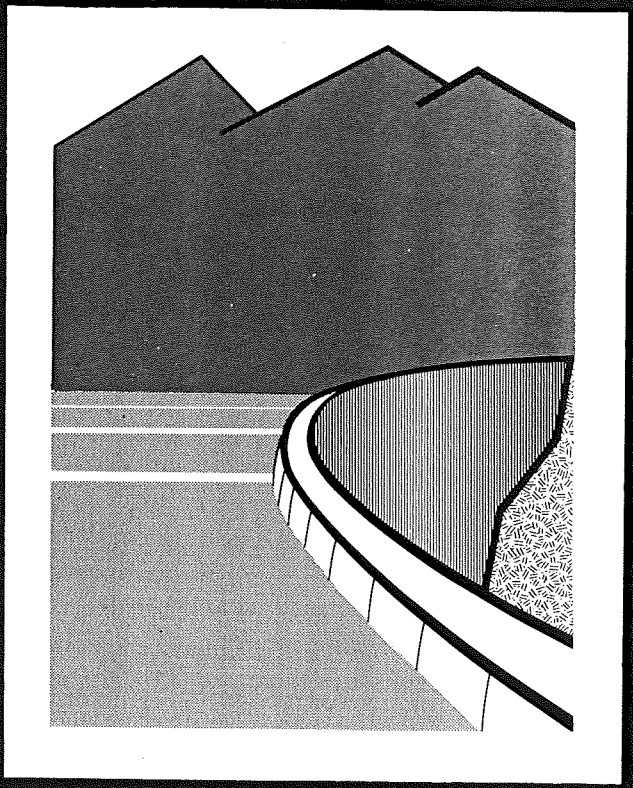

VOLUME 3 ISSUE 1

Numerical analysis of dams with extensive cracking resulting from concrete hydration: simulation of a real case

Miguel Cervera
E.T.S. Ingenieros de Caminos, Canales y Puertos
Universitat Politécnica de Catalunya
Gran Capitán s/n
Barcelona 08034
Spain

Javier Oliver
E.T.S. Ingenieros de Caminos, Canales y Puertos
Barcelona, Spain

Mario Galindo
E.T.S. Ingenieros de Caminos, Canales y Puertos
Barcelona, Spain

SUMMARY

The paper presents the computational model developed to study an existing large gravity dam suffering from observed 'pathological behaviour' resulting from concrete hydration. The combined effect of water intrusion and chemical reactions inside the cement paste produced a deterioration process which motivated experimental and numerical studies. The present study was undertaken to simulate numerically the observed phenomenon and to predict future developments. Concrete is modelled using an isotropic continuum damage model including visco-elastic effects. The triggering of the volumetric expansion resulting from water intrusion is linked to the onset of damage at each point, assuming that water enters the dam mostly through the damaged areas. Transversal construction joints are modelled using smeared joints. Temperature and porewater pressure effects are included using assumed distributions based on available field data. Results are presented which match reasonably well with the available field measurements.

Introduction

Many concrete dams exhibit internal areas of extensive cracking or micro-cracking. Such a situation is unusual for reinforced and pre-stressed concrete structures, where cracking is stricly restricted at design level. The appearance of detectable cracks in such structures is interpreted as a structural failure, and severe security and repair measures are immidiately undertaken. In large structures made of plain concrete, such as dams, a certain amount of cracking and micro-cracking is unavoidable, and the structural analyst should be able to guarantee their overall stability even when large cracked areas exist. The origin of cracks in concrete dams may be found in the phases of design, construction or in operation. The reasons for this cracking may be manyfold: thermal variations caused by internal or external sources, irregular settlements of the foundation, internal chemical reactions during the setting, hardening or ageing of the concrete, seismic actions, and so on. In any case, the onset of cracking increases the ingress of water into the body of the dam. The presence of water inside the

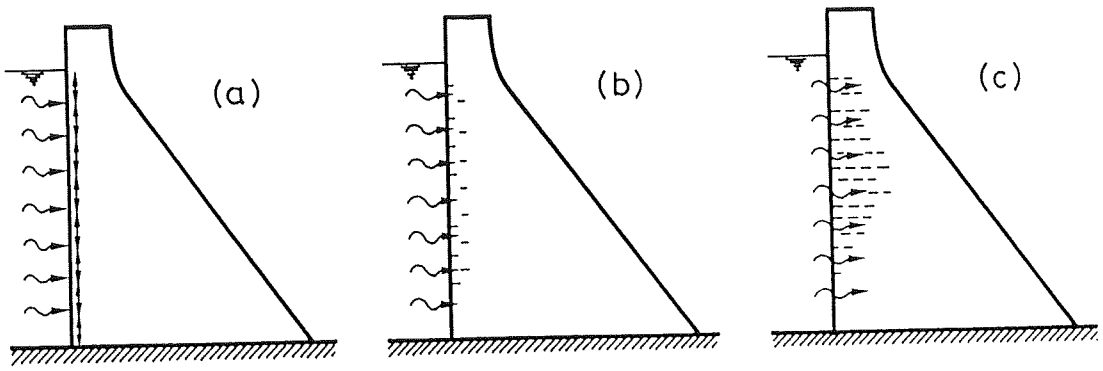

Figure 1. Representation of the phenomenon of water intrusion, concrete hydration and progressive cracking.

dam is quite usual because of seepage. The low permeability of concrete and an effective drainage system should limit the effect of water intrusion. However, the appearance of unexpected cracking and the increased amount of water inside the dam may significantly reduce the safety factor of the structure, in some cases, down to dangerous figures.

Cement contains certain compounds, mainly calcium and magnesium oxides, which combine with water to produce hydroxides. These chemical reactions lead to a significant increase of volume in the mixture. If these changes take place during the setting and hardening of the concrete they will not lead to stresses, and are of no importance. But depending on the production process of the cement these oxides may be present in sizes and densities which greatly retard the hydration reactions, so that they will continue long after the hardening of the concrete. In that situation, the combined effect of water intrusion and concrete hydration may play a paramount role in the propagation of cracking inside the dam. The critical situation which may arise can be described as shown in Figure 1: (a) the concrete in the upstream face is in direct contact with the water in the reservoir. Concrete hydration takes place and the resulting volume expansion induces tensile straining in nearby areas; (b) tensile straining produces the onset of cracking or micro-cracking close to the upstream face. Water enters through these cracks; (c) because of water intrusion, new areas of the dam come in contact with water, and the chemical reactions are triggered. New straining and cracking appears inside the dam. At the same time, the expansion of concrete tends to close the cracks left behind the advancing front of water intrusion.

This process of water intrusion may continue indefinitely, unless an effective drainage system prevents water from reaching further inside the dam. Even in that case, the mass of concrete between the upstream face and the plane of drainage will suffer the described phenomenon, and this will cause important displacements, and most probably, extensive damage and cracking in the dam. The importance of the described process depends mainly on the magnitude of the concrete expansion, and this depends on the physical and chemical properties of the cement. Normal values of the maximum attainable volumetric strain are around 0.3 mm/m, which is comparable with the expected values motivated by seasonal thermal effects. However, values up to 3 mm/m have been measured in some

existing dams, such as the one analysed in this work. These extraordinary values may lead to what can be termed 'pathological behaviour' of the dam: extensive damage occurs inside the structure, and horizontal movements greater than 15 cm. have been measured in some cases.

1 Computational model

The computational model to analyse the sort of process described above is necessarily complex. Let us consider some of the factors contributing to such complexity:

- The mechanical behaviour of concrete is very difficult to model satisfactorily, and many constitutive models have been proposed to such effect. As a result of the long time scale of the problem, the present analysis requires to model both the short and the long term response of the material. Features like fracture under tension, degradation of the elastic stiffness, loading–unloading–reloading, creep and stress relaxation should be taken into account. The use of the Finite Element Method (FEM) allows the consideration of a wide variety of constitutive models: linear and nonlinear elasticity, plasticity, viscoelasticity, viscoplasticity, elastic and plastic damage models, and so on.

- Although gravity dams may be analysed under the plane strain hypothesis, a general computational model should include arch and arch-gravity dams. Analysis by means of the FEM can be readily applied to 2D and 3D problems involving complex geometries and quite arbitrary boundary and loading conditions. However, if any practical 3D study is to be considered, the model should be suitable for large scale computations.

- Large concrete dams are built by blocks, presenting construction joints. These joints may have an important influence in the overall structural behaviour, and so their consideration in the computational model may be necessary. The inclusion of the frictional behaviour of the joints in the analysis is an additional source of nonlinearity, and may present specific difficulties.

- It is necessary for the analysis to simulate the coupled and time-dependant phenomena of water intrusion, concrete hydration and cracking. The physical and chemical processes involved are not yet sufficiently well established as to allow for the analytical solution of such problems. In this work a simplified procedure for the simulation of these phenomena has been used. The validation of such procedure is one of the objectives of this study. It may be added that although the process is time-dependant, its slowness makes it quasi-static, and all time derivatives dependant terms may be neglected.

- There are other effects, such as the seasonal thermal variations and the pore-water pressure, which may affect the dam response. For the particular case considered in this work these effects have little influence when compared to the importance of the volumetric expansion resulting from concrete hydration. Even when these effects are of relevance, they must be considered in an approximate manner, as it is quite unpractical to perform accurate thermal and seepage analyses coupled to the physical-chemical phenomenon described above. Firstly, an enormous ammount of data on enviromental temperature and reservoir levels would be necessary as boundary conditions for both transient problems, and secondly, it is uncertain how concrete hydration may affect the internal distribution of temperature or the permeability of concrete inside the dam.

According to the above considerations the computational model for the finite element simulation of the behaviour of a dam suffering from extensive damage resulting from the hydration of concrete here presented will consider the following items:
(a) a constitutive model for concrete subjected to short term actions;
(b) a modification of the latter to take the long term behaviour into account;
(c) the inclusion of internal actions such as volumetric expansion resulting from hydration, thermal

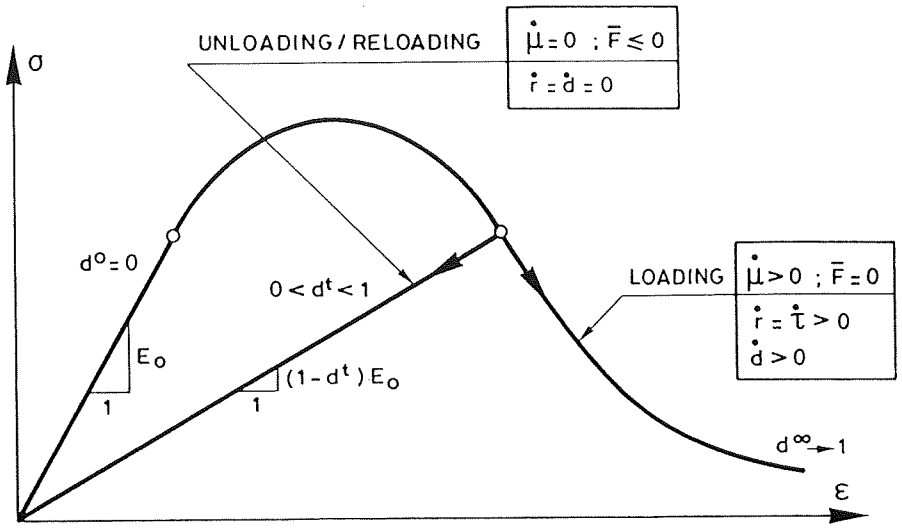

Figure 2. Uniaxial stress-strain curve for damage model.

variations and porewater pressure; and,
(d) a model for frictional construction joints.
It may be added that the proposed model can be readily modified to account for other concrete pathologies not directly connected to water intrusion, such as swelling resulting from alcali-aggregate reaction, for instance.

2 Continuum damage constitutive model for short term behaviour

In recent years, the so-called continuum damage models have been widely accepted as an alternative to deal with complex constitutive behaviour. The approach has proved simple and versatile, and is rigorously based on fundamental constitutive theory. Among the different possibilities that such a framework offers, the simplest is the one referring to isotropic damage models. In these category, non-linear behaviour is monitored through a single internal scalar variable, called *damage* or *degradation*, d. This variable is a measure of the loss of *secant stiffness* of the material, and it ranges from 0 for the undamaged material to 1 for the fully degradated one ($0 \leq d \leq 1$). Figure 2 shows a one dimensional representation of the stiffness evolution of the material.

The model here presented evolves from the work of Simó and Ju [1987] and certain features of the plastic damage model developed by Oller [1988]. The constitutive equation for an isotropic damage model has the simple form:

$$\boldsymbol{\sigma}^t = (1 - d^t)\, \mathbf{D}_e : \boldsymbol{\epsilon}^t \tag{1}$$

where $\boldsymbol{\sigma}^t$ and $\boldsymbol{\epsilon}^t$ are the current stress and strain tensors, respectively; $d^t(\boldsymbol{\epsilon}^t)$ is the damage variable and $\mathbf{D}_e$ is the undamaged constitutive tensor.
Equation (1) reveals some basic features of the model:

- isotropy is preserved, as material stiffness is only affected by a scalar factor;

- explicit integration of the constitutive equation is achieved, as only current values of strain and damage are involved in (1). This makes the model very attractive for large scale computations;
- equation (1) can be also interpreted as an standard additive decomposition of the stress into elastic and inelastic parts,

$$\begin{aligned} \boldsymbol{\sigma}^t &= (1-d^t)\,\mathbf{D}_e : \boldsymbol{\epsilon}^t \;=\; \mathbf{D}_e : \boldsymbol{\epsilon}^t - d^t\,\mathbf{D}_e : \boldsymbol{\epsilon}^t \;=\; \boldsymbol{\sigma}^t{}_e - \boldsymbol{\sigma}^t{}_i \\ \boldsymbol{\sigma}^t{}_e &= \mathbf{D}_e : \boldsymbol{\epsilon}^t \\ \boldsymbol{\sigma}^t{}_i &= d^t\,\boldsymbol{\sigma}^t{}_e \;=\; d^t\,\mathbf{D}_e : \boldsymbol{\epsilon}^t \end{aligned} \tag{2}$$

The model defined by Equation (1) is fully determined if the value of d^t can be evaluated at every time of the deformation process. To that extent one must define:

1. a *suitable norm*, τ^t, of the strain tensor $\boldsymbol{\epsilon}^t$, or alternatively, of the undamaged stress tensor ($\boldsymbol{\sigma}^t{}_e = \mathbf{D}_e : \boldsymbol{\epsilon}^t$). This norm is also called *equivalent strain*, and it is used to *compare* different states of the deformation, so that it is possible to define such concepts as 'loading', 'unloading' and 'reloading'. The norm τ^t is a scalar function with the usual requeriments (i.e. to be positive and to have a zero value for the undeformed state). In section 2.1 some possibilities for the definition of this norm are discussed.

2. a *damage criterion*, $F(\tau^t, r^t) \leq 0$, formulated in the strain or the undamaged stress spaces. The simplest form of this criterion is:

$$F(\tau^t, r^t) = \tau^t - r^t \leq 0 \qquad \forall\, t \geq 0 \tag{3.a}$$

   where τ^t is the norm described in (a), and r^t is the damage threshold at current time t. If r^0 is the initial threshold value (a material property), it must be $r^t \geq r^0$. Expression (3.a) represents a bounding surface in the strain or undamaged stress spaces. Damage occurs when the norm τ^t exceeds the current threshold value, r^t. In particular, damage is initiated when τ^t exceeds for the first time the value r^0. A fully equivalent expression for (3.a), more convenient for this derivation is:

$$\bar{F}(\tau^t, r^t) = G(\tau^t) - G(r^t) \leq 0 \qquad \forall\, t \geq 0 \tag{3.b}$$

   where $G(\cdot)$ is a suitable monotonic scalar function.

3. *evolution laws* for the damage threshold and the damage variable. We define these laws by the rate expressions:

$$\begin{aligned} \dot{r} &= \dot{\mu} \\ \dot{d} &= \dot{\mu}\frac{\partial \bar{F}(\tau, r)}{\partial \tau} = \dot{\mu}\frac{dG(\tau)}{d\tau} \end{aligned} \tag{4}$$

   where $\dot{\mu}$ is a *damage consistency parameter* used to define loading/unloading conditions according to the Kuhn-Tucker relations

$$\dot{\mu} \geq 0 \;\;;\;\; \bar{F}(\tau^t, r^t) \leq 0 \;\;;\;\; \dot{\mu}\bar{F}(\tau^t, r^t) = 0 \tag{5}$$

   From these, it is easy to prove (Simó and Ju [1987]) that the evolution of the internal variables may be explicitly integrated to render:

$$\begin{aligned} r^t &= \max\{r^0, \max \tau^s\} \qquad 0 \leq s \leq t \\ d^t &= G(r^t) \end{aligned} \tag{6}$$

which fully describes evolution of the internal variables for any loading/ unloading/ reloading situation (see Figure 2). Note the simplicity of the resultant algorithm when compared with any smeared crack or plasticity type formulation.

The scalar function $G(\cdot)$ defining the evolution of the damage value must be monotonic, and range from 0 to 1. After some studies it is here proposed the function

$$G(r^t) = 1 - \frac{r^0}{r^t} \exp\left\{ A \left(1 - \frac{r^t}{r^0} \right) \right\} \qquad 0 < r^0 \leq r^t \tag{7}$$

which satisfies the previously stated requirements. Determination of parameter A will be discussed in section 2.2.

2.1 The equivalent strain and the damage criterion

As mentioned above, the norm $\tau(\epsilon)$, together with the damage criterion, plays the important role of defining the *damage bounding surface*. Some possibilities for the definition of such norm were discussed in Oliver *et al.* [1990]. For this work, the equivalent strain τ is defined as

$$\tau = \left(\theta + \frac{1-\theta}{n} \right) \sqrt{\boldsymbol{\sigma}_e : \mathbf{D}_e^{-1} : \boldsymbol{\sigma}_e} \tag{8}$$

where n is the ratio between compressive and tensile strength $n = f_c'/f_t'$ and θ is a weighting factor depending on the state of stress $\boldsymbol{\sigma}_e$. A satisfactory definition of θ is (Lubliner *et al.* [1989]):

$$\theta = \frac{\sum_{i=1}^{3} < \sigma_e^i >}{\sum_{i=1}^{3} |\sigma_e^i|} \tag{9}$$

where $\sigma_e^1, \sigma_e^2, \sigma_e^3$ are the principal undamaged stresses and $< . >$ denotes the McAuly bracket.

The values of θ range from 0 for triaxial compression ($0 \geq \sigma_e^1 \geq \sigma_e^2 \geq \sigma_e^3$) to 1 for triaxial tension ($\sigma_e^1 \geq \sigma_e^2 \geq \sigma_e^3 \geq 0$). For intermediate states $0 < \theta < 1$. Figure 3 shows the corresponding surface $\tau - r^0 = 0$ in the $\sigma_e^1 - \sigma_e^3$ plane and the uniaxial stress-strain curve. It is interesting to note how a simple definition such as that given by Equations (8) and (9) is able to define a bounding surface that approximates reasonably well the observed behaviour of materials such as concrete, both in tension and compression.

2.2 The parameters r^0 and A

Once the function $\tau(\epsilon)$ has been chosen, determination of the initial threshold value r^0 simply requires results from a uniaxial tension test. Substitution of Equation (8) renders:

$$r^0 = \frac{f_t'}{\sqrt{E_e}} \tag{10}$$

Parameter A in Equation (7) is determined as follows. The rate of energy dissipation may be written for all the cases considered as,

$$\dot{\gamma} = \Psi_e \dot{d} = \Psi_e \frac{\partial G(\tau)}{\partial \tau} \dot{\tau} = \Psi_e G'(\tau) \dot{\tau} \tag{11}$$

where $\Psi_e = \dfrac{\sigma_e^2}{2E_e}$ is the free elastic energy.

Therefore, for any process the total specific dissipated energy (per unit volume) is

$$g = \int_0^\infty \dot{\gamma} \, dt = \int_0^\infty \Psi_e \, G'(\tau) \, \dot{\tau} \, dt \tag{12}$$

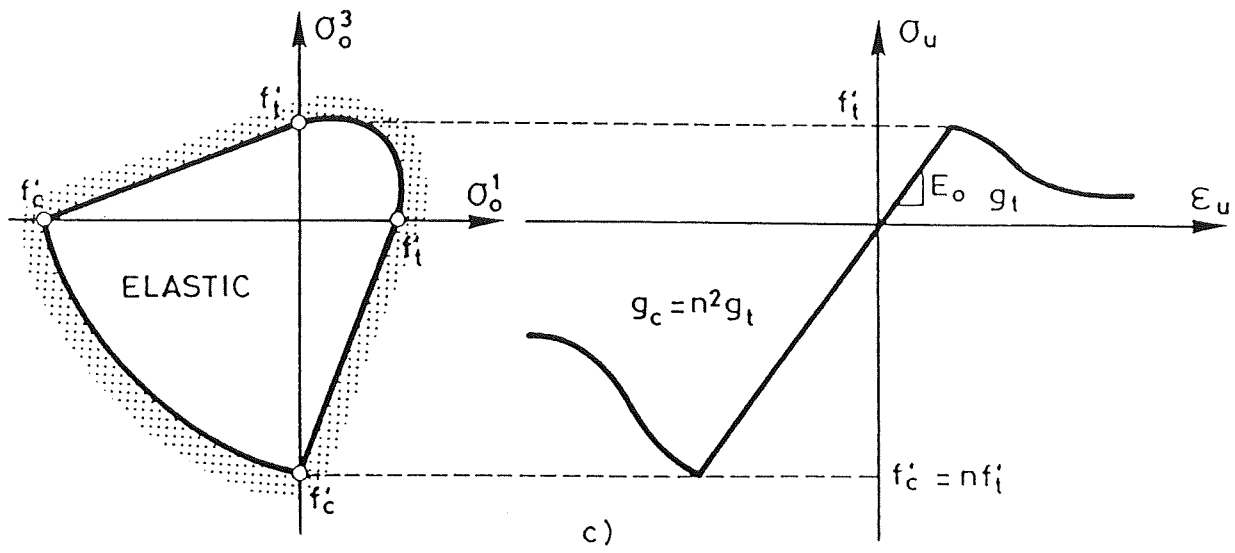

Figure 3. Damage bounding surface and uniaxial curve for the proposed model.

In particular, for the model proposed, it is easy to see that

$$\begin{aligned} \tau^2 &= 2\Psi_e \qquad \text{in uniaxial tension} \\ \tau^2 &= \frac{2}{n^2}\Psi_e \qquad \text{in uniaxial compression} \end{aligned} \tag{13}$$

Substituting the expressions (13) in (12), using the function $G(.)$ defined in (7), and integrating, it yields,

$$\begin{aligned} g_t &= \left(\frac{1}{2} + \frac{1}{A}\right)(\ r^0)^2 \qquad \text{in uniaxial tension} \\ g_c &= \left(\frac{1}{2} + \frac{1}{A}\right)(nr^0)^2 \qquad \text{in uniaxial compression} \end{aligned} \tag{14}$$

where g_t and g_c are the specific dissipated energies in uniaxial tension and compression processes, respectively. Finally, as it is usual in smeared models, it is possible to relate

$$g_t = \frac{G_f}{l^*} \tag{15}$$

where G_f is the fracture energy per unit area (assumed to be a material property) and l^* is a characteristic length of the finite element (Oliver [1989]). Now, from Equations (13), (15) and (10):

$$A = \left(\frac{G_f\ E_e}{l^*(f_t')^2} - \frac{1}{2}\right)^{-1} \geq 0 \tag{16}$$

The value of A in (16) together with the value n in (8) determine the shape of the uniaxial stress-strain curve (see Figure 3). As A must be positive, expression (16) limits the *maximum* size of the element that may be used in a finite element mesh.

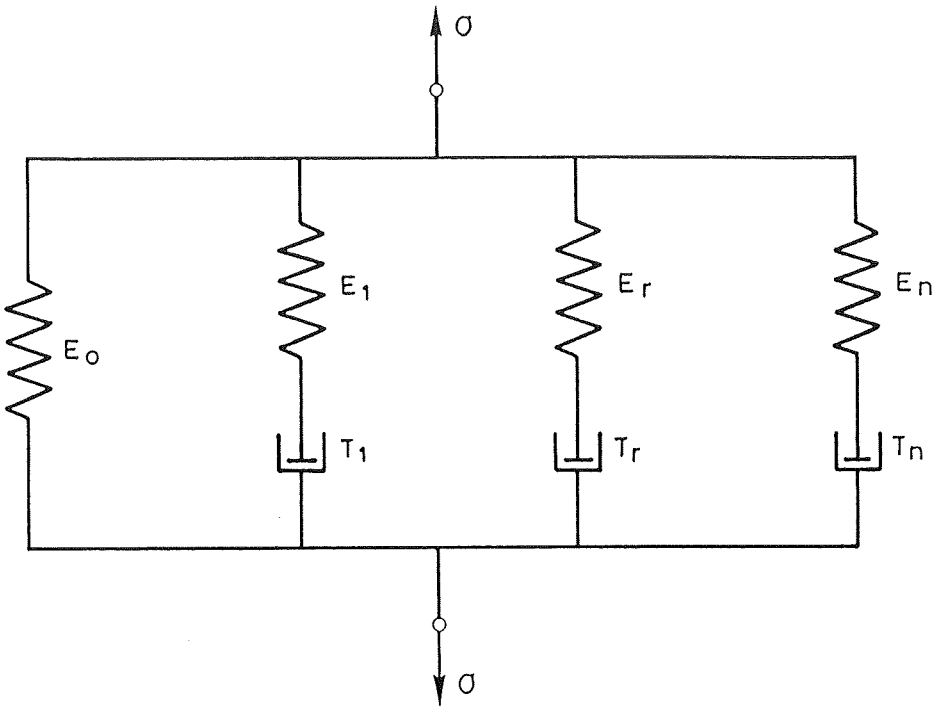

Figure 4. Maxwell chain representing the viscoelastic model.

3 Constitutive model for long term behaviour

Concrete gravity dams are structures subjected to longterm loading and thus, longterm effects such as creep and stress-relaxation may be of importance when modelling their structural behaviour. Creep is usually described in the literature using viscoelastic models. The constitutive laws for viscoelastic materials are formulated via an hereditary integral, which requires memory of the whole strain history. Such an approach is not suitable for numerical applications for obvious reasons. As an alternative, the kernel of the hereditary integral may be expanded as a series with a finite number of terms. Then, the creep process can be described using a finite number of *internal variables*, and only the history of these variables needs to be stored from one time step to the next one (Bažant and Wu [1974], Argyris *et al.* [1977]).

If the hereditary integral is evaluated by parts, and then expanded in a Dirichlet-Prony series, and only a finite number of terms are retained, the resulting model can be mechanically interpreted as a so-called generalised Maxwell chain, where a number of springs and dashpots are arranged in parallel as shown in Figure 4. In this work we will make use of such an arrangement to introduce visco-elastic effects (represented by the dashpots) in the previously mentioned elasto-damaging concrete model (represented by the springs). A similar approach was followed by de Borst [1986] to combine visco-elasticity with a smeared crack model.

For the proposed Maxwell chain, Equation (1) is modified to account for visco-elastic effects:

$$\begin{aligned} \boldsymbol{\sigma}^t &= (1-d^t)\ [\mathbf{D}_e : \boldsymbol{\epsilon}^t \quad - \sum_r \mathbf{q}_r^t] \\ &= (1-d^t)\ [\ E_e \mathbf{D}^* : \boldsymbol{\epsilon}^t \ - \sum_r \mathbf{q}_r^t] \end{aligned} \tag{17}$$

where E_e is the undamaged (elastic) Young's modulus of concrete, $\mathbf{D}^*$ is a tensor representing the Poisson effect for multi–dimensional situations

$$D^*_{ijkl} = \frac{\nu}{(1+\nu)(1-2\nu)}\delta_{ij}\delta_{kl} + \frac{1}{2(1+\nu)}(\delta_{ik}\delta_{jl} + \delta_{il}\delta_{jk})$$

and $\mathbf{q}_r^t$ are *inelastic stresses* caused by the presence of the dashpots in the model. Equation (17) can be rewritten in terms of the *internal stresses* acting on each element of the Maxwell chain:

$$\boldsymbol{\sigma}^t = \boldsymbol{\sigma}_0^t + \sum_r \boldsymbol{\sigma}_r^t$$

with

$$\begin{aligned} \boldsymbol{\sigma}_0^t &= (1 - d^t)\ [\ E_0\ \mathbf{D}^* : \boldsymbol{\epsilon}^t] \\ \boldsymbol{\sigma}_r^t &= (1 - d^t)\ [\ E_r\ \mathbf{D}^* : \boldsymbol{\epsilon}^t - \mathbf{q}_r^t] \end{aligned} \tag{18}$$

where E_0 and E_r represent the initial undamaged stiffnesses of the springs. Comparing Equations (17) and (18), it must be:

$$\mathbf{D}_e \ = \ E_e \mathbf{D}^* \ = \ (E_0 + \sum_r E_r)\mathbf{D}^* \tag{19}$$

Therefore, the initial total stiffness of the concrete is equal to the sum of all the stiffnesses in the Maxwell chain.

For each element in the chain, the following hereditary integral must be evaluated (Cervera *et al.* [1991]):

$$\mathbf{q}_r^t = \int_{t_0}^{t} \frac{E_r}{T_r} e^{-(t-\tau)/T_r}\ \mathbf{D}^* : \boldsymbol{\epsilon}^\tau\ d\tau \tag{20}$$

where T_r is the relaxation time characteristic of each dashpot.

Integration by parts and the assumption that the *internal stresses* defined in (18) vary linearly over each time step allow a recurrence algorithm to be found for the evaluation of the previous integral. It can be shown that the resulting step-by-step algorithm exhibits *cuadratic convergence* The recurrence formula yields,

$$\mathbf{q}_r^t = \gamma_r[1 - \alpha_r(1 - \lambda_r)]\boldsymbol{\sigma}_e^t + \gamma_r[\alpha_r - \lambda_r(1 + \alpha_r)]\boldsymbol{\sigma}_e^{t-1} + \lambda_r \mathbf{q}_r^{t-1} \tag{21a}$$

where

$$\lambda_r = e^{-\Delta t/T_r} \qquad \alpha_r = \frac{T_r}{\Delta t} \qquad \gamma_r = \frac{E_r}{E_e} \tag{21b}$$

and

$$\boldsymbol{\sigma}_e^t = \ \mathbf{D}_e : \boldsymbol{\epsilon}^t \qquad ; \qquad \boldsymbol{\sigma}_e^{t-1} = \ \mathbf{D}_e : \boldsymbol{\epsilon}^{t-1} \tag{21c}$$

Clearly, evaluation of $\mathbf{q}_r^t$ only involves quantities at time $t-1$ and $\boldsymbol{\sigma}_e^t$, which can be readily computed. Thus, only the values $\boldsymbol{\epsilon}^{t-1}$ and $\mathbf{q}^{t-1}$ need to be additionally stored from the previous time step. Figure 5 shows the algorithm that has to be used to evaluate stresses with the proposed model.

Note also that as stress relaxation proceeds, all the strain in each element of the chain is taken by the viscous part of the model (represented by the dashpots in Figure 4), leaving the corresponding elastic stiffnesses (the springs) unstrained. Only the spring with no dashpot connected in series will continue to carry stress. Therefore, after infinite time, only the stiffness $E_0\mathbf{D}^*$ will be active. Most current codes of practice suggest the ratio

$$\frac{E^\infty}{E_e} = \frac{E_0}{E_e} \simeq 0.3 \div 0.6 \tag{22}$$

as appropriate between the apparent stiffness after infinite time and the instantaneous Young's modulus.

INITIAL DATA FOR TIME t

Material properties: $f'_t, n, E_e, \nu, G_f, E_r, T_r$

Current values: $\epsilon^t, d^{t-1}, r^{t-1}, \epsilon^{t-1}, \mathbf{q}_r^t$

1) Determine A (from eq.(16))

2) If $t = 0$ then initialise $r^t = r^0$

3) Evaluate undamaged stresses

$$\sigma_e^{t-1} = \mathbf{D}_e : \epsilon^{t-1}$$
$$\sigma_e^t = \mathbf{D}_e : \epsilon^t$$

4) Evaluate τ^t (from eqn.(8))

5) Update internal variables

$$r^t = \max\{r^{t-1}, \tau^t\}$$
$$d^t = G(r^t)$$

Evaluate $\mathbf{q}_r^t$ from eqn.(21)

6) Update stresses

$$\sigma^t = (1 - d^t)\ [\sigma_e^t - \textstyle\sum_r \mathbf{q}_r^t]$$

Figure 5. Stress evaluation algorithm for damage model with viscoelastic effects.

4 Internal actions

Dams are subjected to several external and internal actions. The main ordinary external actions to be considered are the self-weight and the hydrostatic pressure on the upstream face. Consideration of these loads does not present any difficulty in the numerical simulation. The main ordinary internal actions are the seasonal thermal oscillations and the porewater pressure effect. Other internal actions may have to be considered in particular cases, for instance, the expansion of concrete because of hydration if the maximun attainable volumetric expansion reaches 'pathological' values.

In order to account for the mentioned internal actions, some additional terms have to be considered in Equation (17). The modified expression is:

$$\sigma^t = (1 - d^t)\ [\ \mathbf{D}_e : (\epsilon^t - \epsilon_{hy}^t - \epsilon_{th}^t) - \sum_r \mathbf{q}_r^t\ ]\ - \sigma_p^t \tag{23}$$

where the added terms, ϵ_{hy}^t, ϵ_{th}^t and σ_p^t represented the effects of expansion resulting from hydration, temperature and pore-water pressure at time t, respectively.

4.1 Expansion resulting from hydration

The physical and chemical mechanisms which produce volumetric expansion in concrete in contact with water are very complex and their detailed study lies out of the scope of this work. We will simply assume that a *free extension strain versus time* curve is known for the different parts of the dam (see Figure 6). This curve has to be determined from laboratory tests and *in situ* measurements. If such a curve is known, the corresponding term in (23) can be simply written as

$$\epsilon_{hy}^t = \epsilon_{hy}^t\ \mathbf{I} \tag{24}$$

where $\mathbf{I}$ is the unit tensor and ϵ_{hy}^t is the free extension strain resulting from hydration. In order to evaluate this strain, it is necessary to determine which points of the dam are *wet* at the present time,

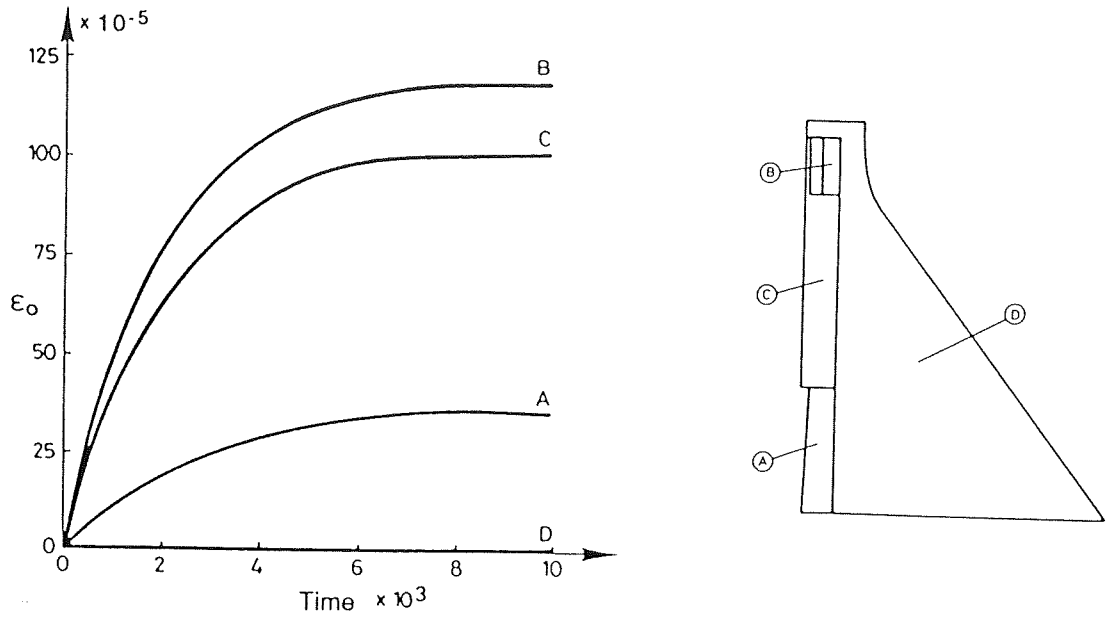

Figure 6. Free expansion strain–vs–time curves for different parts of the dam.

and for how long they have been so. Because of the low permeability of concrete, it is reasonable to assume that water will enter the dam mainly through the damaged (cracked) areas. Accordingly, it will be assumed that each integration point starts tracing its corresponding *expansion strain versus time* curve at the time of onset of damage. Based on these assumptions the simulation process is as follows:

- The analysis begins by considering that, after the application of self-weight and hydrostatic pressure, only those points (elements) adjacent to the upstream face are reached by water and expanding. These points follow their corresponding $\epsilon^t_{hy} - t$ curve from the beginning of the analysis. This imposed deformation will induce increasing tensile strains in the nearby areas.

- When the tensile (and compression) strains and stresses at a certain point (element) exceed the threshold value defined by the constitutive model, degradation is initiated. As assumed above, the expansion process is initiated at the same time and the point starts tracing its corresponding $\epsilon^t_{hy} - t$ curve.

- As more points begin to expand, the process is accelerated and progresses in time. The expansion of concrete induces tensile strains and degradation in the areas located downstream, as well as compression in the areas which are already suffering the expansion. After some time, most of the points located upstream of the drainage plane reach their maximum attainable volumetric strain. The deformation process tends to slow down and, eventually, a steady state may be reached.

As will be shown in the case study, this simple model is able to simulate how water intrusion, concrete hydration and degradation 'travel' from the upstream face to the drainage plane, as it is observed in reality. Areas located downstream of the drainage plane may suffer degradation, but not hydration under the hypothesis of drainage effectiveness. This can be easily simulated assigning null expansion curves to those areas (see Figure 6).

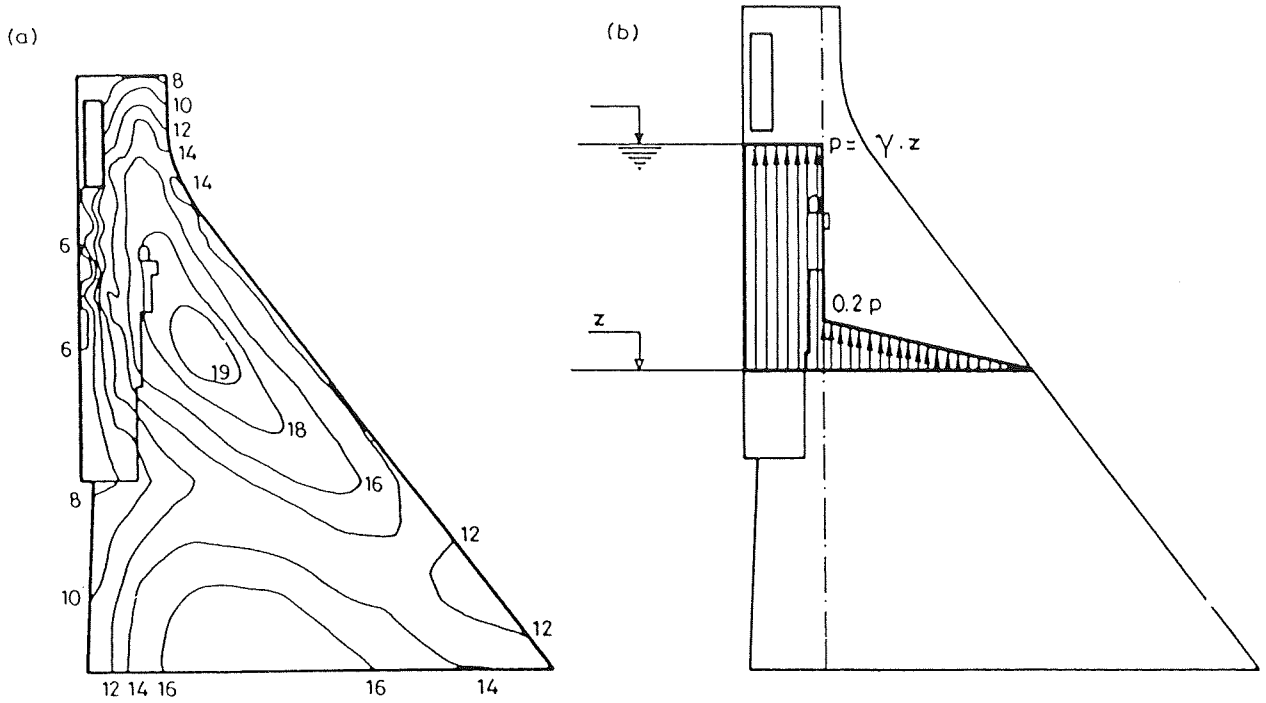

Figure 7. (a) Computed isothermal contours in Spring. (b) Assumed porewater pressure distribution along a transversal line.

4.2 Seasonal thermal oscillations and porewater pressure

Seasonal thermal oscillations produce variations on the volumetric strain in the dam, and therefore, variations on the displacements and stresses. This effect is included in the present work, as thermal straining may force partial or total unloading and reloading on the concrete. Furthermore, differential thermal straining may be an added cause for damage and water intrusion. The thermal effect is included in the analysis through the corresponding term in Equation (23). As the thermal strain is volumetric, it can be written

$$\epsilon_{th}^{t} = \alpha \Delta T^{t} \, \mathbf{I} \tag{25}$$

where $\mathbf{I}$ is the unit tensor, α is the thermal coefficient for concrete and ΔT^{t} is the increment of temperature at time t. To avoid the performance of a coupled thermo-mechanical analysis, a simplified method was adopted to compute the distribution of temperature for each time step. From field data, isothermal contours at different times of a 'typical year' were produced (see Figure 7.a). From these, a mean squares interpolation program was used to fit a sinusoidal curve to define the annual thermal oscillation for each nodal point in a cross-section of the 3D mesh. Then, the same curve was used for all the points along the same longitudinal axis of the dam. These curves, obtained for every nodal point in the mesh, were used to interpolate the corresponding ΔT^{t} terms at the sampling points for every time step during the analysis.

The analysis of a saturated porous medium must be conducted in term of *effective stress*, that is, taking into account the effect of the porewater pressure. This means that in Equation (23) the corresponding term takes the form:

$$\sigma_{p}^{t} = p^{0} \, \mathbf{I} \tag{26}$$

where p^{0} is the porewater pressure and $\mathbf{I}$ is the unit tensor. Again, a simplified method is used to avoid a fully coupled analysis in terms of displacements and pressures. We will simply assume a given

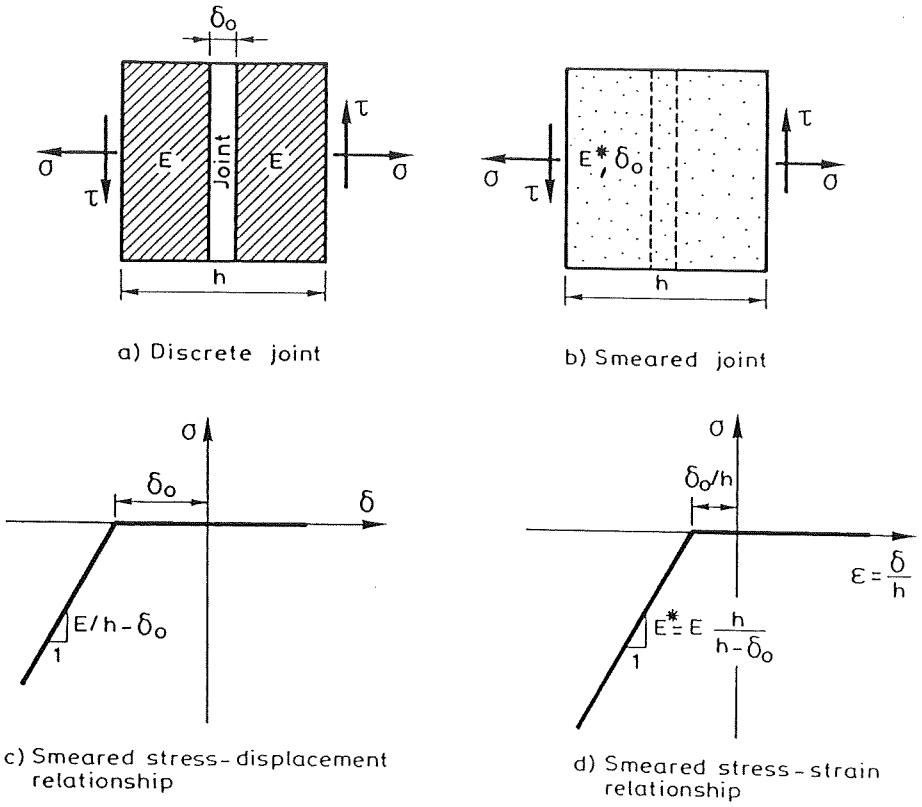

Figure 8. Description of the 'smeared joint' element.

distribution of initial porewater pressure, p^0, over a cross-section of the dam (see Figure 7.b), and use the same nodal pressures along the longitudinal axis. This allows determination of σ_p^t at every sampling point as an initial stress at the beginning of the analysis.

4.3 Construction joints

Large concrete dams present construction joints, and these may influence strongly the structural behaviour. Transversal joints play an important role in a fully 3D analysis, as they allow relative movements between the different blocks of the dam. This effect cannot be simulated in a simplified 2D plane strain analysis. In this work, *smeared joints*, rather than classical discrete joint elements, have been used. Instead of modelling the discrete (dimensionless) joint by itself, it is considered as a part of a composite material which represents the behaviour of the joint and some concrete adjacent to it (see Figure 8). The resulting element has finite dimensions, and relative displacements between its nodes can be interpreted as 'strains' in a standard fashion.

Obviously, the constitutive relations for this *smeared joint material* are orthotropic. Material axes must be fixed in directions normal and tangential to the physical joint, and different behaviour laws must be established for these directions. In the normal direction, a 'no-tension' strain-stress relationship is used. A threshold value can be defined for the compressive strain to simulate the effect of an initial gap in the joint. If this initial gap is not zero, the stiffness modulus in that direction must be corrected, so that when the joint is fully closed the stiffness of the composite material is equal to that of the concrete (see Figure 8). In the tangential directions, a Drucker-Prager elasto-plastic model can be used to simulate the frictional behaviour of the joint, and to relate the normal compression to the maximum shear stress.

It must be noted that even though the use of this smeared model for joints overcomes some of the difficulties inherent to the use of discrete joint elements, it still presents an extremely nonlinear behaviour which results in poor convergence performance in some situations. These aspects must be object of further study.

5 Simulation of a real case: Mequinenza dam

Mequinenza dam, located in Zaragoza province (Spain), is part of the hydroelectric power system of Ebro river. It is a gravity dam 461 m long and 79 m high, with a reservoir of 1530 Hm^3. The different construction blocks have a width of 14 to 21 m, and a central singular one of 70 m, leaving transversal vertical joints in between. Construction took place in the early sixties and regular operation began at the end of 1966. Unexpected downstream movements were observed almost immediately, and cracking and water intrusion was detected, particularly in the central block. These events motivated additional instrumentation and close surveillance of the dam, continued to the present. In Figure 9, a graph of the measured vertical and horizontal movements at the crest in the period 1964–1990 is shown. The *normal* oscillation effect of the seasonal temperature variations can be observed superimposed on an *abnormal* growth of the displacements.

This *pathological* behaviour of the dam motivated a research programme to understand the observed phenomena and to be able to predict the future behaviour of the dam. The study consisted of two phases: firstly, identification and evaluation of the mechanisms involved in the observed phenomena, and secondly, numerical simulation and prediction of the structural response.

It was soon realized that the phenomenon of concrete expansion due to hydration was mostly responsible for the problem. Qualitative studies and laboratory tests showed that the composition of the concrete used in the Mequinenza dam, and especially in the central block, were such that volumetric strains resulting from hydration could reach values up to 3 mm/m. This is about one order of magnitude bigger than the volumetric strains resulting from thermal loading. The second stage of the study was undertaken to simulate the observed behaviour, evaluating the state of the dam and the extension of the internal damage. The results presented below correspond to the conclusions of this second stage.

Figure 10 shows the 3D finite element mesh used for the analysis (1056 20-noded elements, 16764 degrees of freedom). The model includes the central block, located between the construction joints termed J13 and J14, and some adjacent blocks. The mesh is chosen so that appropriate boundary conditions for the central block can be simulated. Figure 11 shows a cross-section of the dam in which the elements which begin to expand from the start of the analysis (those in the upstream face) can be distinguished from the elements which begin to expand at the onset of damage. Downstream of the drainage plane no expansive behaviour is considered. The stabilization time for the free expansion versus time curves has been established in 192 months (16 years).

5.1 Qualitative results

Figure 12 shows different views of the deformed shape of the dam at the end of the analysis (the displacement amplification factor is fifty). The last plot corresponds to the deformed shape of the central cross-section. It can be seen that concrete expansion produces an uplift movement, together with a downstream rotation. These effects are evident for the upper part of the central block. Differential movements of the central block relative to the lateral ones produce sliding of the construction joints, and thus, these must be adequately modelled.

Figures 13 and 14 show contours of the scalar damage variable, from a downstream view and on the central crosssection, respectively. It can be seen that damage occurs mostly in the upper/central part and in the drainage plane (interface between the areas accesible and non-acccesible to water). The obtained movements and damage contours correspond well to the expected deformation mode: the expansive areas tend to move upwards and are restrained by the rest of the dam, where tensile straining is induced.

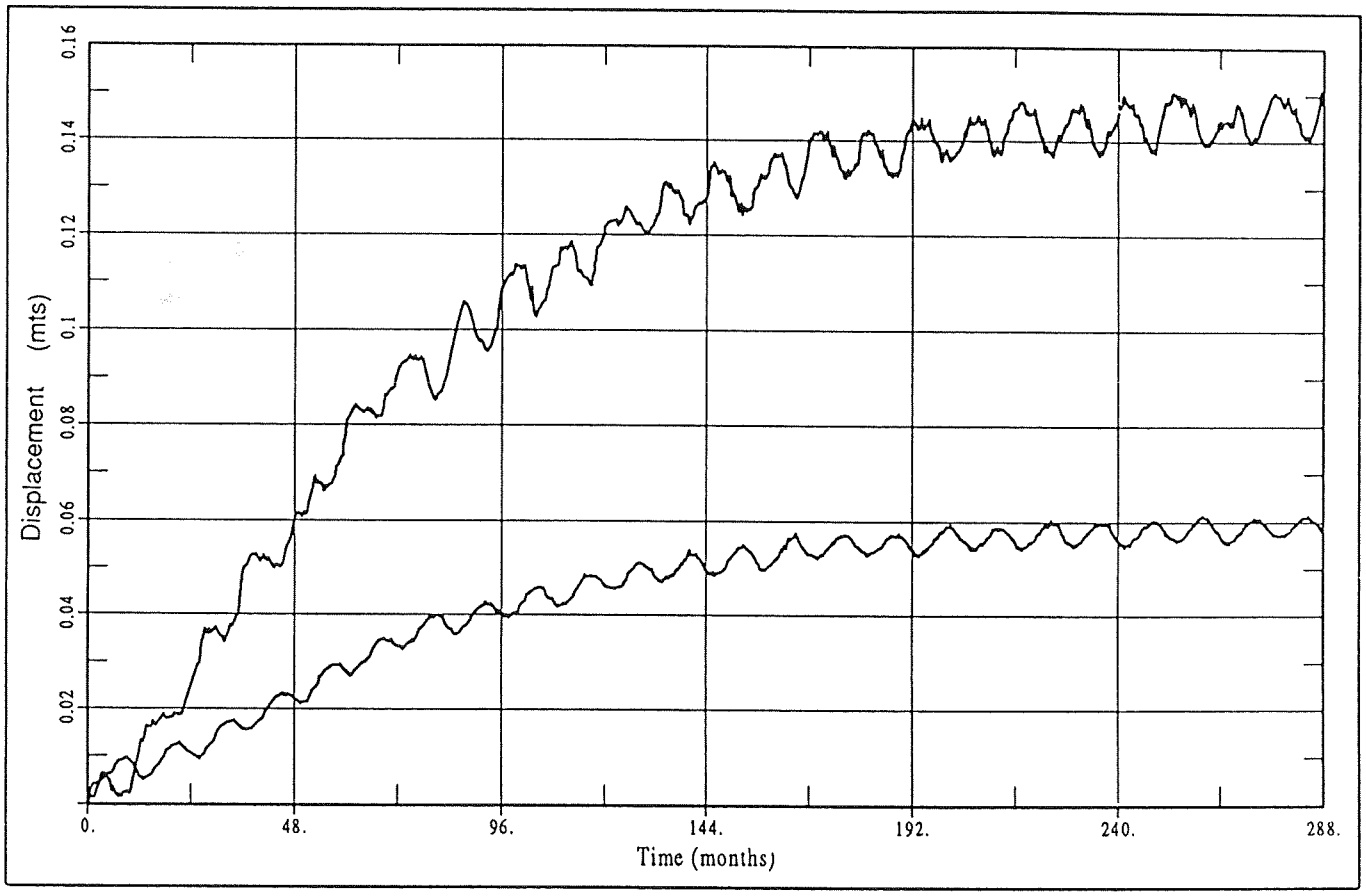

Figure 9. Measured vertical and horizontal movements at the crest.

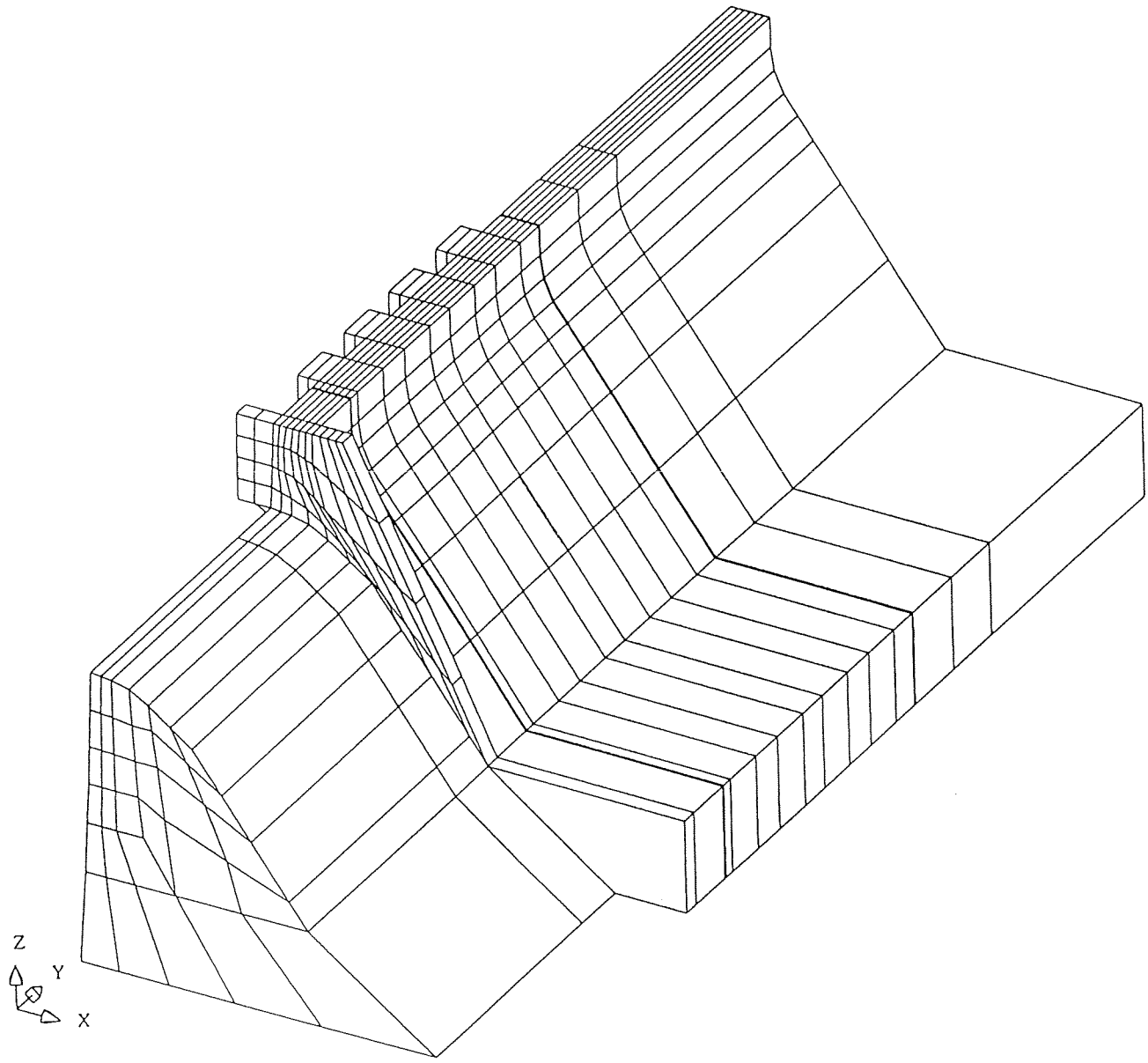

Figure 10. Finite element mesh.

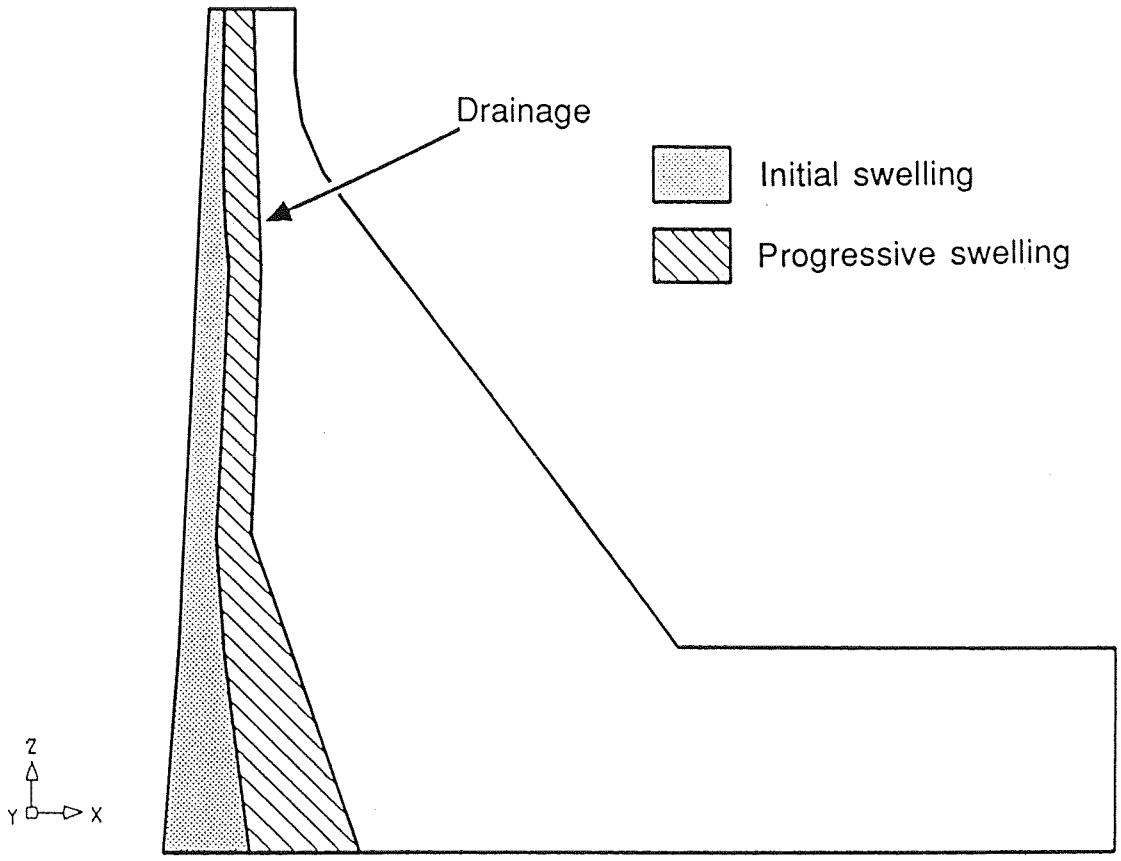

Figure 11. Initial and progressive expansion areas.

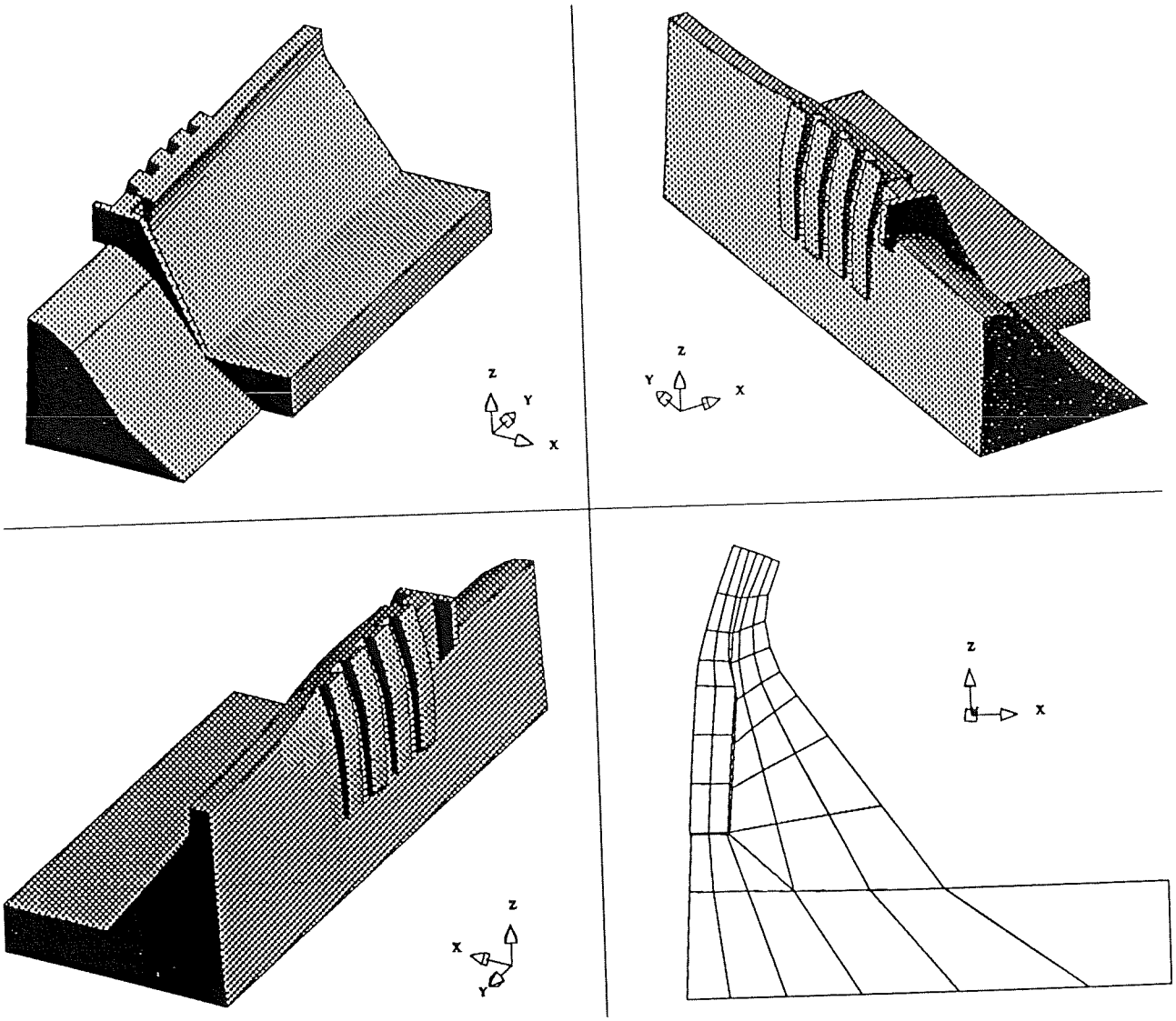

Figure 12. Views and central cross-section of the deformed shape of the dam.

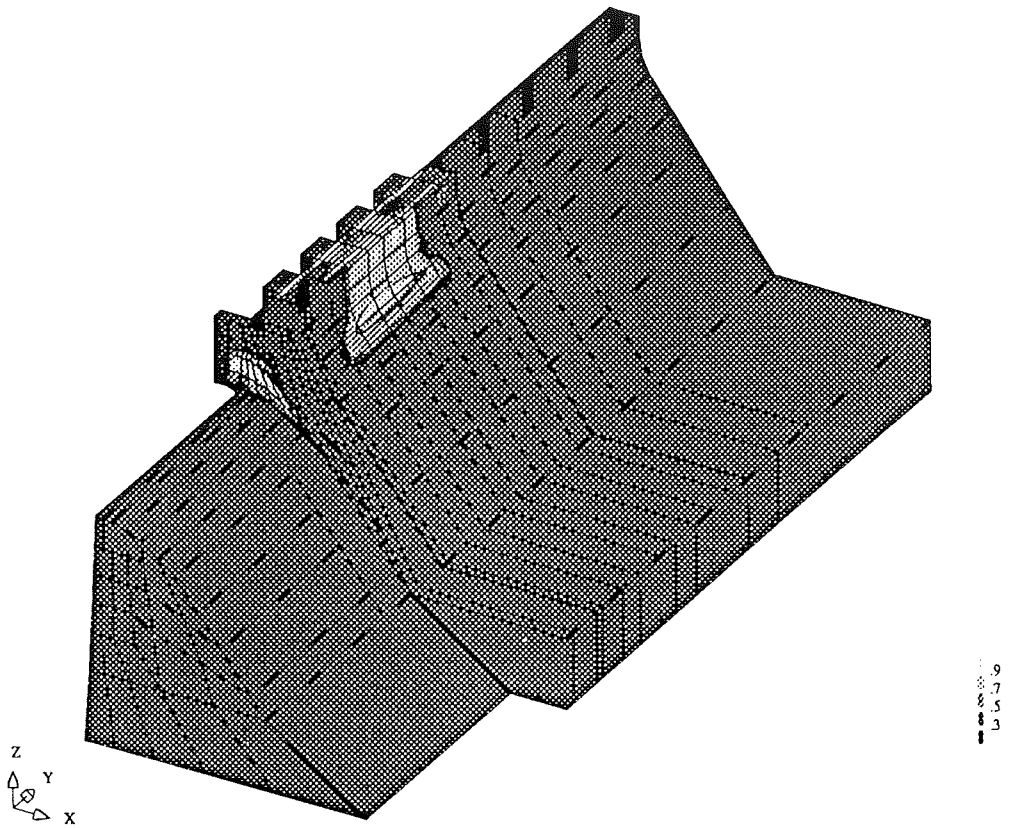

Figure 13. Damage contours. Downstream view.

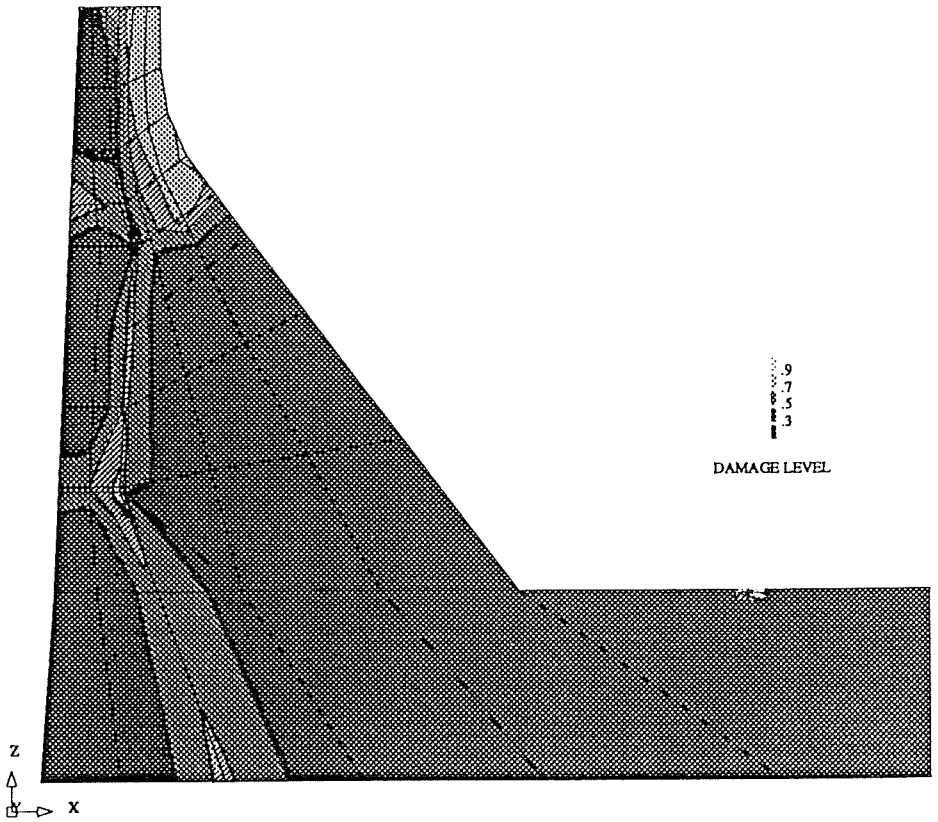

Figure 14. Damage contours. Central cross-section.

5.2 Quantitative results

Figure 15 shows the comparison between computed and measured displacements, for the year 1990. The first figure shows the lines along which the comparison is made. Lines L1 and L2 (crest) are used to compare displacements along the axes X and Z, respectively. Line L3 (downstream) is used to compare the longitudinal displacement (axis Y). In the other figures the solid lines represent the computed deformed shape of the corresponding line and the crosses represent the maximum and minimum values measured during 1990. Good agreement can be found for the three plots, where the sliding of the joints can also be compared with the measurements. Figure 16 shows the time history of the downstream displacement (axis X) for point P1 (crest, see Figure 15), from 1966 to 1990. Computed results are shown without the thermal oscillations for the sake of clearness. Agreement between the numerical simulation and measument is good. Stabilization is reached for a maximum horizontal displacement around 15 cm.

Conclusion

The main conclusion of this study is that concrete hydration, and its progression towards the interior of the dam (as a consequence of water intrusion) is able to explain, by means of the computational model developed, the observed abnormal behaviour in some large concrete dams. The agreement between the obtained results and the field measurements corresponding to the case study of Mequinenza dam assesses the validity of the simulation.

Acknowledgements

The authors gratefully acknowledge the help received from OCIDE through the national *Plan de Investigación Electrotécnica* (P.I.E.).

Bibliography

ARGYRIS J.H., PISTER K.S., SZIMMAT J. AND WILLAM K.J., "Unified concepts of contitutive modelling and numerical solution methods for concrete creep problems", *Comp. Meth. App. Mech. Engn.*, 10, pp. 199-246; 1977.

BAŽANT Z. P. AND WU S.T., "Rate–type creep law for aging concrete based on Maxwell chain", *RILEM Materials and Structures*, 7, pp. 45-60; 1974.

CERVERA M., OLIVER J. AND GALINDO M., "Simulación Numérica de Patologías en Presas de Hormigón", *CIMNE report*, No. 4; 1991.

DE BORST R., "Computational aspects of smeared crack analysis" in "Computational Modelling of Reinforced Concrete Structures", *Book*, Ed. Hinton E. and Owen R., Pineridge Press; 1986.

LUBLINER J., OLIVER J., OLLER S., AND OÑATE E., "A Plastic-damage Model for Concrete", *International Journal on Solid Structures*, 25, pp. 299-326; 1989.

OLIVER J., "A Consistent Characteristic Length for Smeared Cracking Models", *International Journal for Numerical Methods in Engineering*, 28, pp. 461-474, 1989 .

OLIVER J., CERVERA M., OLLER S. AND LUBLINER J., "Isotropic damage Models and Smeared Crack Analysis of Concrete", *Proceedings*, II Int. Conf. on Computer Aided Analysis and Design of Concrete Structures, Ed. N. Bicanic and H. Mang, Pineridge Press; 1990.

OLLER S., "Un modelo de daño contínuo para materiales friccionales", *Ph. D. Thesis*, E.T.S. Ingenieros de Caminos. Universidad Politécnica de Cataluña; 1988.

SIMO J. C. AND JU J. W., "Strain– and Stress–based Continuum damage Models - I. Formulation", *International Journal on Solid Structures*, 23, pp. 821-840; 1987.

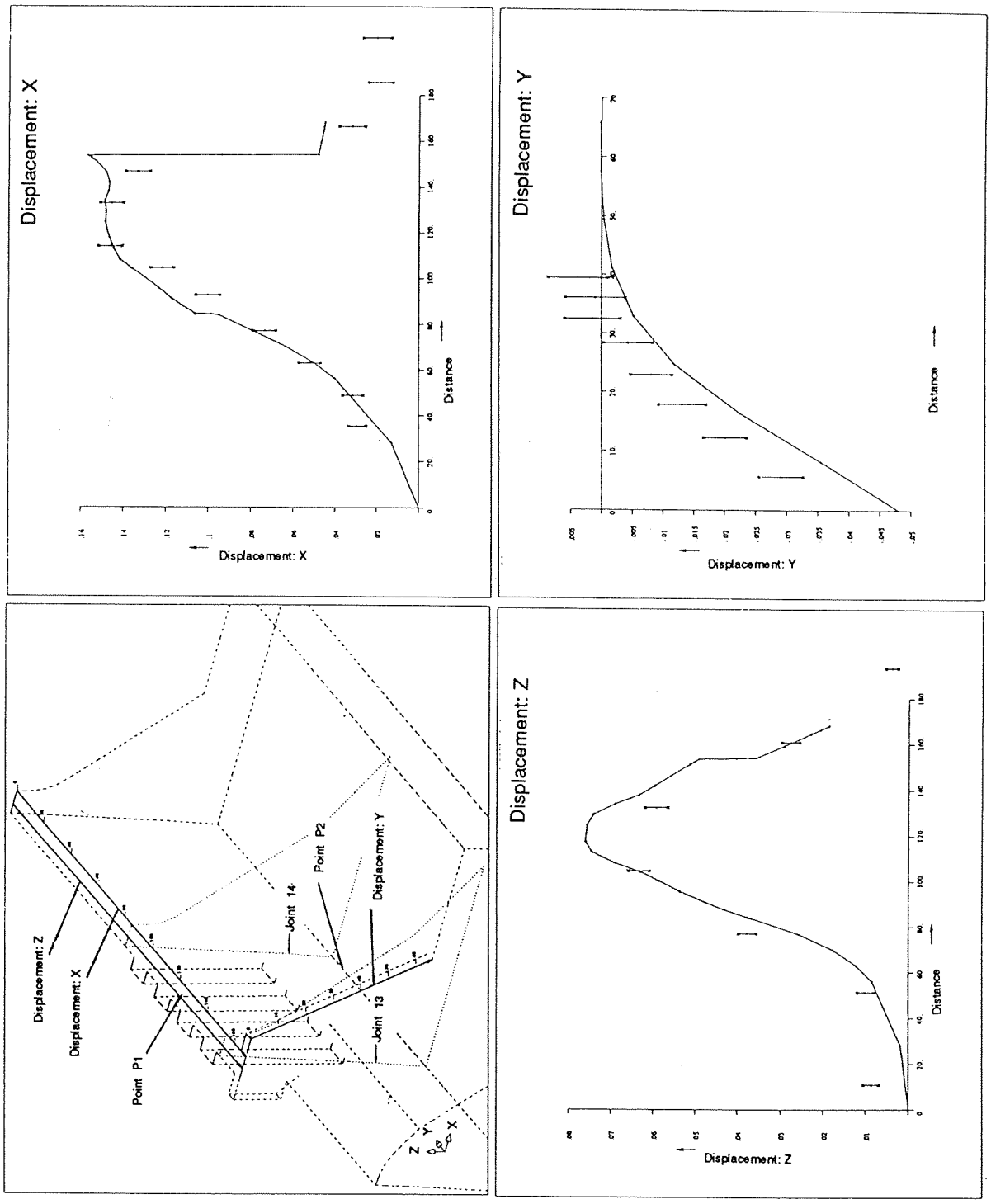

Figure 15. Comparison between displacements computed and measured for the year 1990.

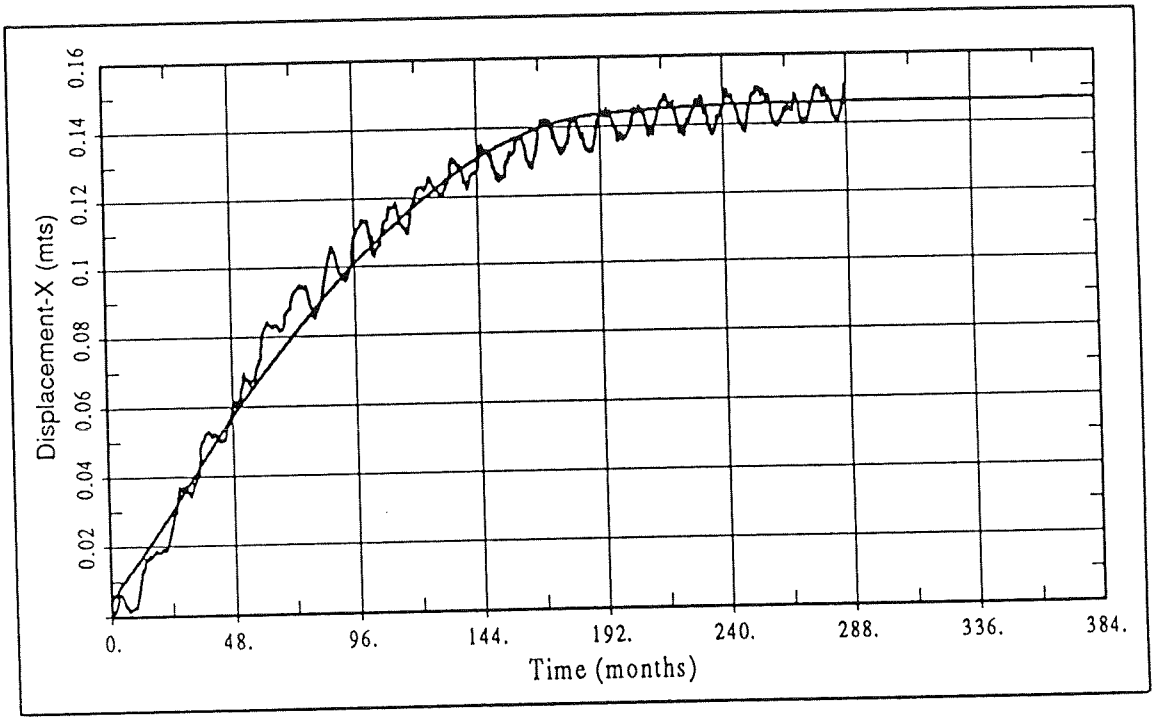

Figure 16. Comparison between computed and measured displacements X (P1: crest).